Biophysical Chemistry 144 (2009) 1–8

Contents lists available at ScienceDirect

Biophysical Chemistry

journal homepage: http://www.elsevier.com/locate/biophyschem

Binding interactions in early- and late-stage amyloid aggregates of $TTR_{(105–115)}$ ☆

Yanfang Liang [a], Shohreh Zahedi Jasbi [a], Sina Haftchenary [a], Sylvie Morin [a], Derek J. Wilson [a,b,*]

[a] York University, Department of Chemistry, Toronto, ON, Canada M3J 1P6
[b] Center for Research in Biomolecular Interactions, Toronto, ON, Canada M3J 1P6

ARTICLE INFO

Article history:
Received 2 March 2009
Received in revised form 13 May 2009
Accepted 18 May 2009
Available online 22 May 2009

Keywords:
Amyloidosis
Saturation transfer
Nuclear magnetic resonance
Aggregation
Transthyretin
Atomic force microscopy

ABSTRACT

One of the central aims of amyloid research is to identify chemical and structural features that confer amyloidogenic propensity. In this study, we use Saturation Transfer Difference (STD) NMR spectroscopy to acquire an atom-specific map of the interactions between soluble and aggregated Transthyretin peptide ($TTR_{105–115}$) in early- and late-stage amyloidogenesis. Atomic Force Microscopy (AFM) was used to monitor the transition of early-stage samples, containing protofilaments, to late-stage samples composed of fully-mature fibrils. Progressive aggregation was accompanied by an increase in the correlation time τ_c of soluble $TTR_{105–115}$ as indicated by ^{1}H NMR line broadening, but no significant change in the ^{1}H chemical shifts. The STD profile of backbone amide protons is in good agreement with an earlier computational study predicting hydrogen bonding propensity for each residue in small $TTR_{105–115}$ aggregates (Paci et al., J. Mol. Biol. (2004) 555–569). The STD profiles of C_α and C_β protons identify a central aliphatic region of the peptide, Ala108–Leu111, that plays a crucial, but different role in early- and late-stage amyloidogenesis. In general, the STD profiles of early and fully-mature samples are dissimilar, suggesting different mechanisms of self-assembly in protofilaments and mature amyloid fibrils. The early-stage mechanism appears to be more dependent on main-chain hydrogen bonding, while the late-stage mechanism involves an increased number of interactions between bulky side chains.

1. Introduction

Amyloidosis is a pathogenic form of protein aggregation that has been implicated in over 40 human illnesses, including Alzheimer's, Parkinson's, type II diabetes and Creutzfeldt–Jakob disease [1,2]. Mature amyloid fibrils share a common stacked cross β-sheet structure [3], but the mechanisms by which this structure is adopted varies considerably from protein to protein [4]. Moreover, it is not clear if the interactions that govern the formation of pre-amyloid intermediates are the same as those that enable the incorporation of additional subunits into mature amyloid fibrils [5]. Elucidation of amyloidogenic mechanisms can provide a basis for the rational design of drugs targeting obligatory intermediates in the amyloidogenic process.

Transthyretin (TTR) amyloidosis is the most common hereditary systemic protein aggregation disease [6]. Amyloidogenic propensity in human TTR is promoted by an 11 residue peptide, $TTR_{105–115}$ (sequence Y-T-I-A-A-L-L-S-P-Y-S), which corresponds to a β-strand in the native protein structure [7,8]. $TTR_{105–115}$ readily forms amyloid-like fibrils in vitro under a range of conditions and is therefore a convenient model for fundamental studies on the mechanisms of amyloid formation. It is also one of a small number of amyloidogenic species whose atomic level structure in mature amyloid fibrils has been elucidated using a set of *intra*molecular distance constraints [9,10], providing a detailed account not only of the backbone conformation, but also the precise positions of the side chains.

Solution phase Nuclear Magnetic Resonance (NMR) is a powerful tool for studying early amyloid aggregation processes [11–13]. It cannot be used, however, to investigate mature fibrils directly due to their extremely long correlation times. Solid state magic angle spinning NMR has been used to obtain atomic resolution structures of monomers within mature fibrils [9,10,14]. Saturation transfer difference NMR spectroscopy was originally designed to detect the binding of small molecule ligands to protein targets [15,16]. In this experiment, nuclei on the large binding partner are saturated by sustained, selective irradiation, avoiding direct saturation of ligand resonances. Saturation spreads rapidly within the large molecule, and can be transferred to the ligand through binding. Intermolecular saturation transfer can occur through multiple binding events during the saturation period, creating a pumping effect that boosts the sensitivity of the experiment [16]. In addition, *intra*molecular saturation transfer is slow in small molecules, preserving preferential saturation of those atoms most associated with

☆ This work was supported by the Canada Foundation for Innovation (CFI) and the Ontario Research Fund (ORF), the Natural Science and Engineering Research Council (NSERC) and York University.

* Corresponding author. York University, Department of Chemistry, Toronto, ON, Canada M3J 1P6. Tel.: +1 416 736 2100x20786; fax: +1 416 736 5936.
E-mail address: dkwilson@yorku.ca (D.J. Wilson).
URL: http://www.yorku.ca/dkwilson (D.J. Wilson).

0301-4622/$ – see front matter © 2009 Elsevier B.V. All rights reserved.
doi:10.1016/j.bpc.2009.05.007

binding [17]. Thus, it is possible to 'map out' binding interactions on the ligand.

STD NMR was first applied to amyloid systems by Narayanan et al. in 2003 [18] and again in 2005 to study chemical exchange in the Alzheimer's associated Aβ-amyloid under variable salt conditions [19]. Milojevic et al. used STD NMR to elucidate the interactions underlying inhibition of Aβ oligomerization by human serum albumin [20]. These investigations centered on early and intermediate amyloidogenic states. In this work, we use STD NMR to contrast binding interactions in protofilaments and fully-mature amyloids of $TTR_{105-115}$. Our aim is to provide a detailed rationale for amyloidogenic propensity in this peptide and to identify any differences that may exist in the mechanisms that govern early- and late-stage amyloidogenesis.

2. Experimental

2.1. Materials

All peptides were directly dissolved in HPLC grade water (Sigma, St. Louis MO) containing 10% (v/v) CD_3CN and 0.1% (v/v) TFA, both of which were supplied by ACP chemicals (Montreal, QC). 10% (v/v) D_2O was added for NMR calibration (Sigma). The final pH was 1.9. Bradykinin was supplied by Sigma and $TTR_{105-115}$ was synthesized by Celtek peptides (Nashville, TN). 700 µL, 1-µM peptide solutions were filtered using 0.2 µm nylon syringe filers (Fisher Canada, Ottawa, ON) and collected directly into 5-mm Norell NMR tubes (Chemglass, Vineland, NJ) for analysis. Samples were allowed to age at 25 °C for approximately 3 weeks, during which time NMR analyses were conducted and aliquots were removed periodically for AFM experiments.

2.2. Atomic force microscopy

All AFM images were recorded under dry conditions. $TTR_{105-115}$ amyloid solutions were applied to a freshly cleaved mica substrate and allowed 30 min for adsorption. The substrate was then rinsed with the HPLC grade water and dried with Argon gas which was purchased from Air Liquide (Burlington, ON). Imaging was carried out in tapping mode using a Dimension 3100 Scanning Probe Microscope (SPM) from Veeco (Peabody, MA). Tapping mode images (512 × 512 pixels) were obtained using 125-µm silicon SPM tip with a spring constant of 37.09 N/m which was purchased from Digital Instruments (Santa Barbara, CA). A scan speed of 1.00 Hz, drive amplitude of 200–973.4 mV and resonant frequency of 298–300 Hz were employed. The scan sizes ranged from 2 × 2 to 15 × 15 µm.

2.3. NMR spectroscopy

All of the NMR experiments were performed at 25 °C on Bruker DRX 600 MHz Spectrometer. Water suppression was achieved using excitation sculpting with gradients [21]. All 1D ^1H NMR experiments were recorded with 128 scans, 16 dummy scans and spectral width of 6.6 kHz. Data were processed and analyzed using the MestRe Nova program (Mestrelab Research, Santiago de Compostela, Spain).

2.4. Diffusion Ordered NMR Spectroscopy (DOSY)

DOSY experiments were carried out to measure diffusion coefficients $D = (k_B T)/(6\pi\eta F r_s)$ where r_s is the hydrodynamic 'stokes' radius, F is the Perrin factor, η is the sample viscocity, k_B is the Boltzmann constant and T is the absolute temperature. In DOSY experiments, the z-axis position of the analyte is recorded in a gradient echo. The relative signal intensity I/I_0 changes with respect to the parameters of the gradient echo according to the expression:

$$\frac{I}{I_0} = e^{-D(\Delta-\delta/3)q^2} \quad (1)$$

where D is the diffusion coefficient, Δ is the gradient echo spacing, δ is the duration of the gradient, and $q = \gamma\delta g$ where γ is the gyromagnetic ratio and g is the gradient strength. Varying one of these parameters (usually g) while holding the others constant gives a signal decay curve that is recorded in the F1 axis and fit to expression (1) to give D. In our experiments, the parameters were $\Delta = 35$ ms, $\delta = 2$ ms and 16 values of g between 5% and 100% of 33 G/cm. Diffusion coefficients were extracted using the dsFit script for NMRPipe [22].

2.5. 2D NMR spectroscopy

All 2D NMR experiments were carried out with spectral widths of 6.6 kHz in both dimensions. Quadrature detection was by States-TPPI with 2048 points in the direct dimension for each of 64 increments in the indirect dimension. The use of low resolution in the indirect dimension was necessary to minimize the experiment time on samples that were actively undergoing fibrilization. To obtain an acceptable level of signal-to-noise, up to 512 transients were collected per increment. Typical experiment times were 12 h, while the first TTR protofilaments were observed by AFM at ~24 h. TOtal Correlation SpectroscopY (TOCSY) spectra were acquired using the DIPSI-2 sequence for mixing [23]. The isotropic mixing time was 80 ms. NOESY and ROESY experiments used mixing times between 50 and 175 ms. NOESY mixing times of up to 250 ms were tried for early-stage samples without enhancement of the observed NOEs.

2.6. STD NMR

STD experiments were carried out as described previously [16]. Selective saturation was achieved using a train of 60 Gaussian-shaped pulses at 40 dB and 12-ms duration separated by a 1-ms delay. Longer pulse trains increased total saturation of soluble $TTR_{105-115}$ somewhat, but reduced preferential saturation at specific sites, likely due to increased time for *intra*molecular saturation transfer. Saturation transfer reference (STR) spectra were acquired with off-resonance irradiation at 25 ppm. Saturation transfer experiments were conducted with on-resonance irradiation at 0 ppm, a value selected to maximize saturation of the amyloid fibrils without direct saturation of free $TTR_{105-115}$ (see Results and discussion). The number of scans and dummy scans in the STD experiments were 128 and 16, respectively. Saturation transfer efficiency was measured as the ratio of the intensity of the on- and off-resonance difference spectrum I_{STD} to the off-resonance spectrum I_{STR} at each peak. To compare classes of protons, I_{STD}/I_{STR} values were normalized to the highest STD efficiency $I_{STD}^{max}/I_{STR}^{max}$ within that class [20]. The low pH conditions allowed amide protons to be included in the analysis as proton exchange with solvent was very slow relative to the experiment. Peak intensity measurements were made using the MestRe Nova software.

3. Results and discussion

3.1. Time-dependent analysis of fibril morphology

AFM was used to provide a quantitative picture of the time-dependent increase in fibril concentration and size over the maturation period. Fig. 1 shows AFM images $TTR_{105-115}$ fibrils at various stages of maturation from when the first filamentous aggregates (exclusively protofilaments) were observed (Fig. 1A, 24 h) to full maturation (Fig. 1D, 3 weeks). The fibrils exhibit an 'unbranched strand' morphology consistent with that reported in the literature [24]. The estimated cross-sectional areas, ranging from 115 nm^2 for protofilaments to 321 nm^2 for mature fibrils, are also in agreement with literature measurements [7,24,25], although we observe a flatter, wider shape which is likely the result of differing adsorption conditions. A typical width measurement is shown in Fig. 1F. The main morphological difference between fully-mature $TTR_{105-115}$ fibrils and their 'younger'

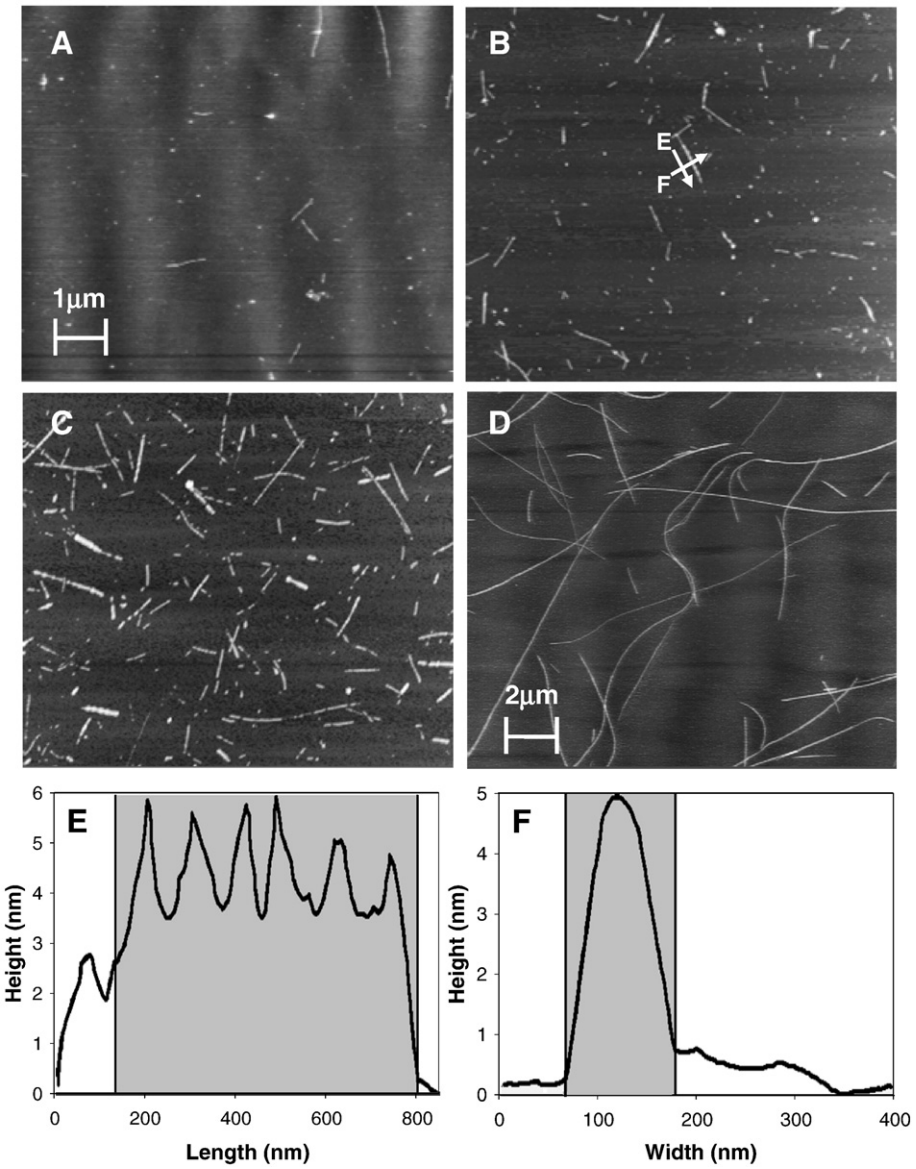

Fig. 1. AFM images of $TTR_{105-115}$ at various ages. (A) 24 h, (B) 60 h, (C) 78 h, and (D) 3 weeks. Panel A contains only protofilaments, panels B and C include a mixture of protofilaments and amyloid fibers and panel D shows only mature fibrils. Panel E represents a continuous height measurement along the length of a typical fibril (white arrow marked E in panel B), which clearly shows a series of protrusions and indents with ~100-nm spacing. A representative width measurement is shown in panel F.

counterparts appears to be length; we observe an average 'fully-mature' length of 8.2 μm ± 0.05 compared to 753 nm ± 7 in early samples [24,25]. This observation supports the generally accepted model for amyloid growth as occurring via elongation only, such that new subunits are incorporated exclusively at the fibril ends.

Fibrils are adsorbed onto the mica substrate individually and do not appear to form bundles as has been previously reported [24], however, a number of fibril pairs are observed in a tightly wound configuration. Close examination of some maturing fibrils reveals a periodic substructure of protrusions and indents occurring approximately every 110 nm along the fibril length (Fig. 1E). This observation is in line with the generally accepted picture of amyloid fibrils as consisting of a twisted bundle of protofilaments [26]. Interestingly, the substructure appears more strongly in younger protofilaments and less strongly in fully-mature fibrils. This may reflect a process by which fibrils become more tightly wound as they age, reducing the size of the 'twist' protrusions and indents to below the resolution of our AFM experiments.

3.2. 1D and 2D NMR spectroscopy

Fig. 2 shows ^{1}H NMR spectra from early-stage (A) and fully-mature (B) $TTR_{105-115}$ samples. Diffusion Ordered Spectroscopy (DOSY) measurements indicated that the peaks in the early-stage ^{1}H NMR spectrum (Fig. 2A) arise from a species with diffusion coefficient $D \approx 5 \times 10^{-9}$ m^2 s^{-1}. Based on the correlation between D and peptide molecular weight [27], this value is consistent with the TTR monomer, being comparable to that for peptides with MW around 1200 Da (*e.g.* α-conotoxin II, MW 1352 Da, $D = 4.22 \times 10^{-9}$ m^2 s^{-1}) but significantly higher than peptides with MW around 2400 Da (*e.g.* endothelin-III, MW 2643, $D = 3.01 \times 10^{-9}$ m^2 s^{-1}).

As samples aged, however, exponential fits to the DOSY signal decay profiles became increasingly poor, indicating a loss of the exponential relationship between I/I_0 and D. One possible cause is increasing sample viscosity, which accompanied fibrilization to the point where fully-mature samples were completely gelled. In 'non-ideal', polymer containing solutions, the Stokes–Einstein relationship between D and

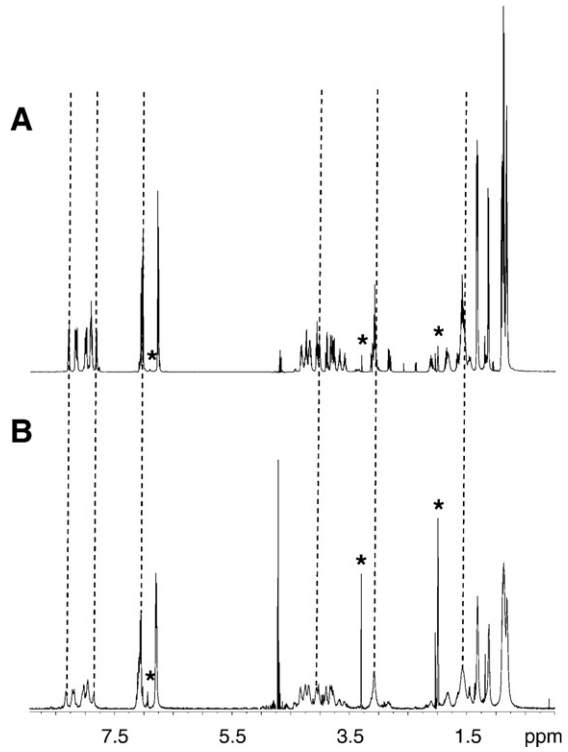

Fig. 2. 1D spectra from early-stage and fully-mature (gelled) TTR samples. (A) Early stage. (B) Fully mature. The signal is greatly reduced in fully-mature samples due to the incorporation of the majority free $TTR_{105-115}$ into fibrils. Lines are significantly broader but the chemical shifts do not change appreciably (dotted lines). Peaks marked with '*' represent small molecule contaminants whose absolute intensity is the same in early and mature sample spectra. Both spectra were recorded at 600 MHz and 25 °C in 0.1% (v/v) TFA and 10% CD_3CN (pH 1.9).

r_s, upon which the analysis of DOSY NMR data ultimately relies, does not hold [28]. Thus, DOSY experiments provide good evidence that the observed species in early-stage samples is a monomer, but do not shed light on the nature of the observed species in late-stage samples.

Fully-mature samples were invariably gel phase, but gave reasonable ^{1}H NMR spectra nonetheless, indicating the presence of a soluble $TTR_{105-115}$ species within the fibril gel matrix. It is tempting to argue, based on the broader lineshapes in the fully-mature spectrum (Fig. 2B), that the observed species in late-stage samples is an oligomer, however, in a gel sample, line broadening might as easily result from limited motional freedom within the fibril gel matrix, transient interactions with the fibrils or B_0 field heterogeneity. As emphasized by the dotted lines in Fig. 2, the chemical shifts in late-stage samples are unchanged from early-stage samples. On the assumption that oligomerization would result in at least a small change in the observed chemical shifts, we can tentatively argue that the species observed in late-stage samples is the same as the species observed in early-stage samples (*i.e.* a monomer).

^{1}H chemical shifts were assigned using TOtal Correlation SpectroscopY (TOCSY), Nuclear Overhauser Effect SpectroscopY (NOESY) and Rotating frame nuclear Overhauser SpectroscopY (ROESY). Early-stage samples gave good TOCSY spectra with NH/αH, NH/βH and NH/γCH_3 correlations even at relatively low mixing times (Fig. 3A). The quality of TOCSY spectra diminished with sample maturation, likely due to the increasing transverse relaxation rate, such that reasonable TOCSY spectra could not be obtained from fully-mature, gelled samples. Early-stage samples exhibited very poor NOEs because the correlation time of $TTR_{105-115}$ monomers τ_c lies within a range that is not conducive to efficient cross relaxation [29]. It was therefore necessary to conduct ROESY experiments to unambiguously assign the peptide from early-stage samples only.

Fully-mature samples exhibited strong, negative NOEs (Fig. 3B) even at short mixing times (<100 ms) giving the expected direct correlations (*i.e.* NH/[α-1]H), a number of correlations likely to arise purely from spin diffusion (*i.e.* NH/γCH_3) and correlations that may have significant contributions from both (*i.e.* NH/αH and NH/βH). The appearance of strong, negative NOEs is indicative of an increased τ_c for the observed species of $TTR_{105-115}$, which may be taken as evidence for oligomerization, but, as with our earlier observations, may also reflect restricted motional freedom within the fibril gel matrix. Extensive peak overlap and spin diffusion preclude the extraction of reliable distance constraints from the data. A rudimentary Chemical Shift Index analysis using the αH resonances [30] predicts a random coil configuration, suggesting that the observed species of $TTR_{105-115}$ does not conform to the expected structure in an amyloidogenic oligomer (*i.e.* a stacked β-sheet).

Taken together, the conventional NMR data are suggestive, but not conclusive, of a monomeric amyloidogenic subunit of $TTR_{105-115}$ in both early- and late-stage amyloidogenesis. An assembly of monomers is consistent with the most recently proposed mechanism of amyloidogenesis for full-length TTR [26]. Confirmation of this hypothesis may be possible with the application of a more advanced DOSY-based analysis as introduced very recently by Baldwin et al. [31].

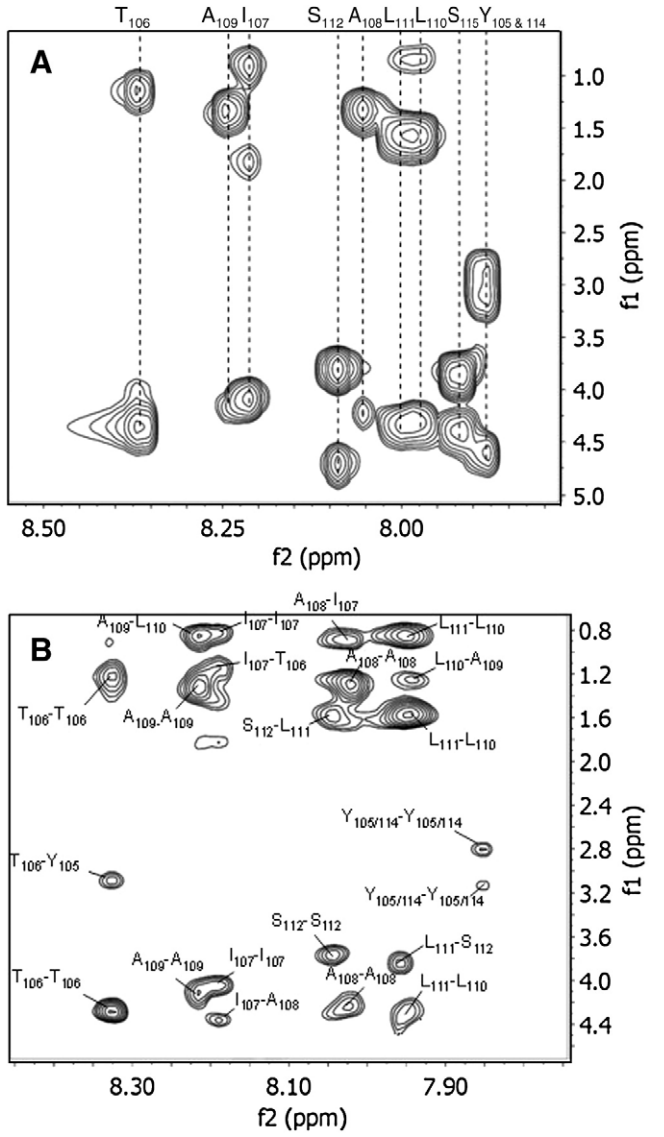

Fig. 3. Fingerprint region 2D NMR spectra of early and fully-mature (gelled) $TTR_{105-115}$ samples. (A) TOCSY of an early-stage sample with residue assignments. (B) An assigned NOESY from a late-stage sample. Many strong, negative peaks are observed even for the intermediate (120 ms) mixing time shown. Both spectra were recorded at 600 MHz and 25 °C in 0.1% (v/v) TFA and 10% CD_3CN (pH 1.9).

3.3. Saturation transfer difference NMR spectroscopy

STD experiments require careful placement of the 'on-resonance' saturation pulse to maximize saturation of the large binding partner without directly saturating the ligand. Previous STD studies on amyloid systems have placed the selective saturation pulse around 0 ppm, which is well upfield of methyl proton resonances from soluble $TTR_{105-115}$, but still excites a fraction of amyloid methyl protons due to their much broader range of chemical shifts [19]. In order to ensure that there was no direct saturation of free $TTR_{105-115}$ in our experiments, we placed our selective saturation pulse at various positions around 0 ppm. Values above 0.3 ppm resulted in direct saturation of Leu110 and Leu111 methyl protons (located at ~0.9 ppm). Transferred saturation was not observed when the saturation pulse was placed below −2 ppm. It was therefore decided that saturation pulse placement at 0 ppm offered maximum saturation of $TTR_{105-115}$ amyloid resonances without risking direct irradiation of free $TTR_{105-115}$.

Fig. 4 shows STD spectra (red) together with their respective 'off-resonance' reference spectra (cyan) for Bradykinin, early-stage and fully-mature $TTR_{105-115}$ samples. Bradykinin, a neuropeptide (R-P-P-G-F-S-P-F-R) which does not form amyloids under our experimental conditions, was used as a negative control (Fig. 4A). No significant saturation transfer was observed from this sample at any time. Weak saturation transfer was observed from early-stage $TTR_{105-115}$ samples (Fig. 4B) indicating the presence of a small population of aggregates undergoing dynamic exchange with free $TTR_{105-115}$. Stronger saturation transfer was detected in fully-mature samples of $TTR_{105-115}$ (Fig. 4C), which is consistent with a larger population of amyloid fibrils in dynamic exchange with free subunits.

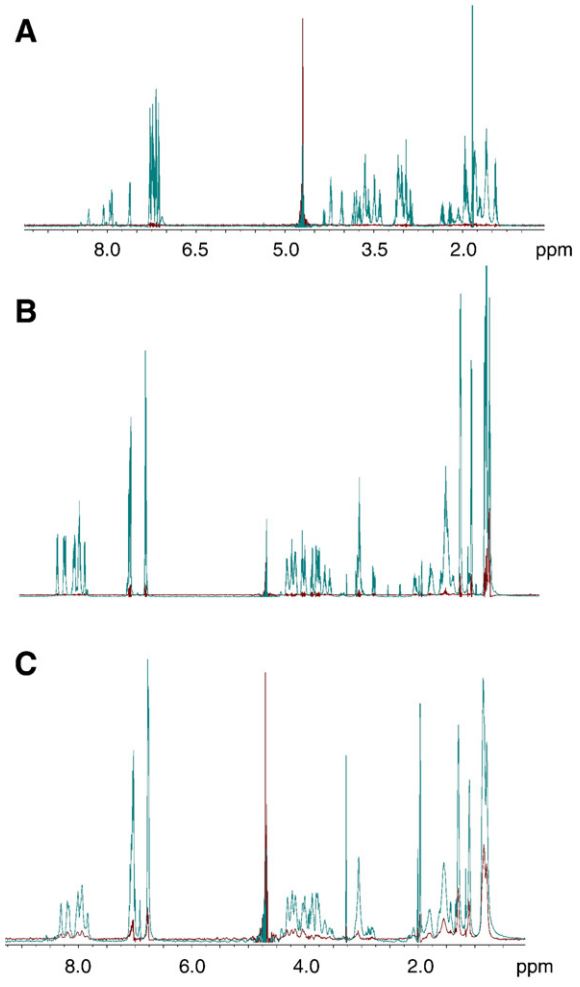

Fig. 4. STD spectra of Bradykinin (A), early-stage (B) and fully-mature $TTR_{105-115}$ (C) together with their off-resonance reference spectra. STD spectra are shown in red, reference spectra in cyan. (A) Bradykinin was used as a negative control. No significant transferred saturation was observed from this sample. (B) Saturation transfer is weak in early-stage samples of $TTR_{105-115}$, but the signal-to-noise was nonetheless sufficient to extract an STD profile. (C) Much stronger saturation is observed in the fully-mature $TTR_{105-115}$ sample. All spectra were recorded at 600 MHz and 25 °C in 0.1% (v/v) TFA and 10% CD_3CN (pH 1.9). (For interpretation of the references to color in this figure legend, the reader is referred to the web version of this article.)

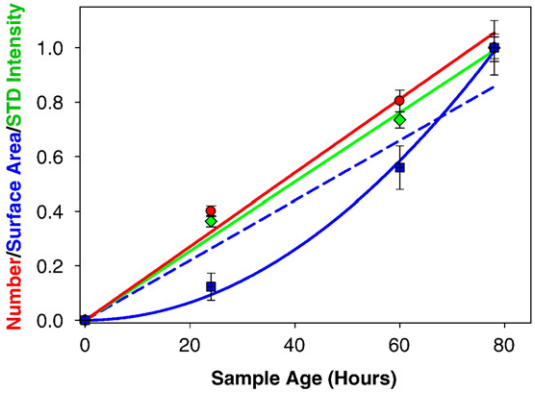

Fig. 5. Time-dependent increase in the number of fibrils (red), total fibril surface area (blue) and STD signal intensity (green). The relative number of fibrils and total fibril surface area were determined from the average of 4 AFM images per time-point. STD intensities were acquired by integrating three 'representative' I_{STD}/I_{STR} ratios, averaged over 5 data sets per time-point. Time-dependent increases in the number of fibrils and STD signal intensity were well described by linear fits to the data (solid red and solid green lines, respectively), while the increase in total fibril surface area was not (dashed blue line). The increase in surface area A was better fit to the non-linear expression $A(t) = t^{1.5}$ (solid blue line). (For interpretation of the references to color in this figure legend, the reader is referred to the web version of this article.)

An additional control experiment was devised to ensure that the observed saturation transfer was related to specific interactions occurring at the growing fibril ends rather than non-specific interactions with the fibril surface. The experiment relies on the fact that for a given system, the overall STD intensity I_{STD} is proportional to the number of interactions [16,32]. In the early stages of amyloidosis, when fibrils are predominantly in the protofilament stage, the number of *specific* interactions will correlate *only* with the number of fibrils (*i.e.* each fibril presents two terminal binding sites, regardless of length). Thus, as the number of fibrils increases over time, there will be a corresponding increase in I_{STD}. Conversely, if the STD signal were to arise from non-specific interactions anywhere on the fibril surface, its intensity would correlate with the total fibril surface area (*i.e.* the number of interactions would be length and diameter dependent). The increase in I_{STD} over time would therefore be a function both of fibril number *and* average size.

Fig. 5 compares the number of fibrils (red) and total fibril surface area (blue), as determined from AFM data, to I_{STD} (green) at different time-points in early amyloidogenesis. In order to compare the growth rates on the same *y*-axis, each data set has been normalized to its respective highest value. The number of fibrils increases linearly (solid red line) over the first 78 h of amyloidogenesis. Growth in the total surface area is non-linear, which is expected given that the fibrils are increasing both in number and in size. The time-dependent increase in I_{STD} correlates much better with the number of fibrils than the total available surface area, indicating that the STD signal results from specific interactions at the fibril ends.

3.4. Saturation transfer profiles

Atom-specific saturation transfer profiles are shown in Fig. 6. The left column represents early-stage samples, while the right column shows profiles from fully-mature samples. Rows correspond to classes of atoms: Backbone amide protons are at the top, the middle panes

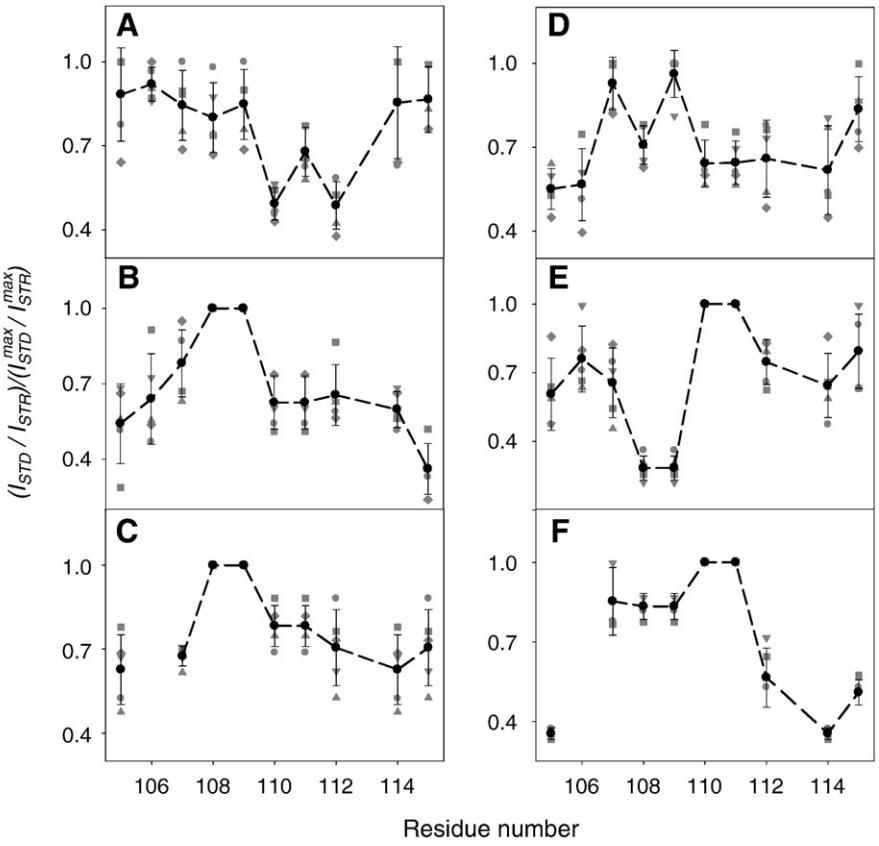

Fig. 6. Relative saturation transfer efficiency profiles as a function of residue number for early-stage (A, B, C) and fully-mature (D, E, F) $TTR_{105-115}$ samples. Classes of protons are delineated by Row: Panels A and D correspond to backbone amide protons, panels B and E correspond to C_α protons, while panels C and F denote C_β protons. The reported ratio $(I_{STD}/I_{STR}) / (I_{STD}^{max}/I_{STR}^{max})$ represents the observed saturation (normalized to a reference peak where the saturation was placed at 30 ppm) as a percentage of the highest saturation signal for a given stage-of-sample and proton class. Black circles are averages of five replicates (which are shown in grey).

correspond to C_α protons while the bottom panels show C_β protons. A first look at the data reveals an important general result: The STD profiles from early- and late-stage samples are *dissimilar*, indicating that the interactions governing the formation of early $TTR_{105-115}$ aggregates are not the same as those governing the incorporation of free $TTR_{105-115}$ subunits into mature fibrils. More specific insights can be acquired by considering each class of atom separately in the context of the role that it might play in binding.

While the STD profile of backbone amide protons does not represent direct evidence of hydrogen bonding, close proximity of backbone amides to the fibril upon binding would suggest an increased likelihood of intermolecular hydrogen-bond formation. In general, the early-stage amide profile (Panel A) shows a higher number of amide hydrogens in close proximity to the fibril, suggesting that the early-stage binding mechanism is more hydrogen-bond dependent. Panels A and D identify two residues, Ile107 and Ala109, whose amides are always in close proximity to the fibril on binding. The late-stage profile in particular shows a striking pattern in which the Ile107 and Ala109 amide protons are highly saturated, while saturation of the Ala108 amide proton is significantly lower. This result is in exact agreement with an experimentally constrained molecular dynamics study by Vendruscolo et al. who predicted the probability of hydrogen-bond formation during a 5 ms $TTR_{105-115}$ self-assembly simulation [5]. The 'on/off/on' pattern of hydrogen bonding in Ile107–Ala108–Ala109 was predicted to be associated with an in-register, antiparallel arrangement. Amide protons on Leu110, Leu111 and Ser112 are generally less saturated in early- and late-stage profiles, this time with the early-stage profile showing an 'on/off/on' pattern.

Saturation profiles for C_α and C_β protons are broadly similar to each other, but there are significant differences when comparing the early- to late-stage profiles. Early-stage profiles indicate that C_α and C_β protons on Ala108 and/or Ala109 (the peaks are fully overlapping) are in closest proximity to the fibril on binding, whereas these same protons are the *least* saturated in the late-stage C_α proton profile. In late-stage samples, the C_α and C_β protons in closest proximity to the fibril are Leu110 and/or Leu111. These protons show only moderate saturation in early-stage samples. In general, the C_α and C_β profiles are suggestive of a central aliphatic region that plays a critical, but different role in binding in early- vs. late-stage aggregates of $TTR_{105-115}$. A similar central aliphatic region was identified from samples of $A\beta_{12-28}$ in their interactions with human serum albumin [20].

Fig. 7 provides a schematic depiction of the proximity data acquired in our STD experiments for early- (A) and late-stage (B) amyloidogenesis, assuming an in-register antiparallel arrangement. Dashed lines do not represent confirmed hydrogen bonds, but rather close proximity on binding which we interpret as a high probability of intermolecular main-chain hydrogen-bond formation. Side chains with high relative proximity on binding (defined as $\geq$70% of maximum saturation on both C_α and C_β protons) are circled. In general, the picture that emerges is of an early-stage mechanism of $TTR_{105-115}$ self-assembly that is dominated by main-chain hydrogen bonding and a late-stage mechanism that involves an increased number of aliphatic contacts interactions.

4. Conclusions

We have acquired an atom-specific map of the interactions between soluble and aggregated $TTR_{105-115}$ in the early and late stages of amyloidosis. Control experiments were carried out to ensure that the observed STD profiles were a result of specific, amyloidogenic

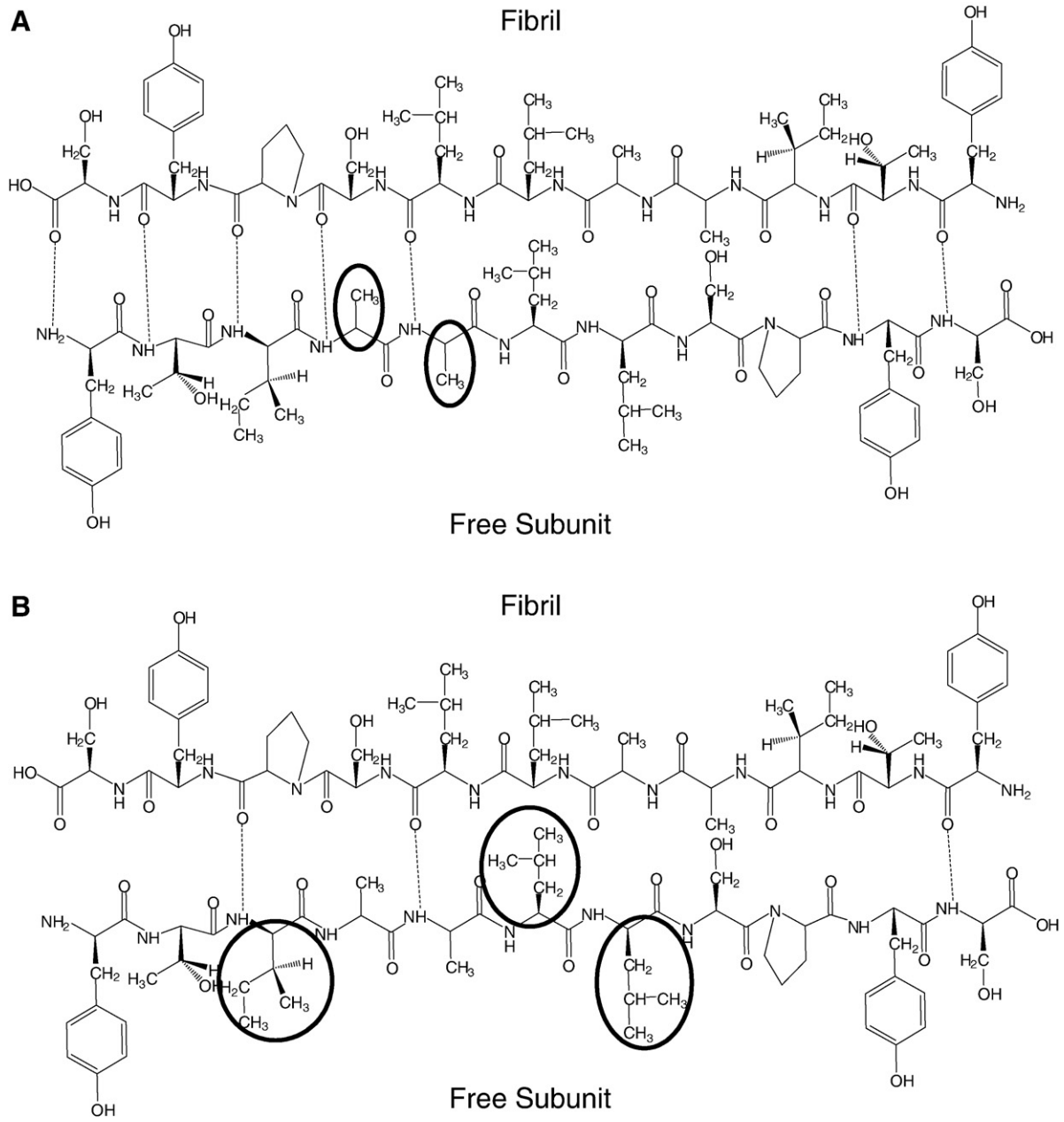

Fig. 7. A schematic depiction of the interactions governing early and late-stage amyloidosis as suggested by the proximity data, assuming in-register inter-strand hydrogen bonding. Backbone amides in close proximity to the fibril on binding are interpreted as a high probability of 'in register' hydrogen bonding with carbonyls on the fibril (dotted lines). Side chains that are in close proximity to the fibril on binding are circled. (A) Early stage. (B) Late stage.

interactions. In broad terms, the STD profiles suggest that the interactions underlying the growth of protofilaments are not the same as those governing the incorporation of additional $TTR_{105–115}$ subunits into mature fibrils. In keeping with our long term objective of identifying characteristics associated with amyloidogenic propensity, future work will examine the impact of mutations and small molecule inhibitors on $TTR_{105–115}$ morphology and amyloidogenic interactions. Based on our current results, it may be possible to rationally design $TTR_{105–115}$ mutants that readily form protofilaments but not fully-mature amyloid fibrils. We are currently undertaking a time-resolved analysis of fibril growth using solution phase, real-time AFM and STM.

Acknowledgements

We thank Xavier Salvetalla, Chris Waudby and Andy Baldwin for providing expert advice on STD and DOSY experiments. We gratefully acknowledge Howard Hunter for technical help with the NMR instrument and helpful discussions.

References

[1] R.W. Carrell, D.A. Lomas, Conformational disease, Lancet 350 (1997) 134–138.
[2] M.B. Pepys, Amyloidosis, Annu. Rev. Med. 57 (2006) 223–241.
[3] R. Nelson, M.R. Sawaya, M. Balbirnie, A.O. Madsen, C. Riekel, R. Grothe, D. Eisenberg, Structure of the cross-beta spine of amyloid-like fibrils, Nature 435 (2005) 773–778.
[4] F. Bemporad, G. Calloni, S. Campioni, G. Plakoutsi, N. Taddei, F. Chiti, Sequence and structural determinants of amyloid fibril formation, Accounts Chem. Res. 39 (2006) 620–627.
[5] E. Paci, J. Gsponer, X. Salvatella, M. Vendruscolo, Molecular dynamics studies of the process of amyloid aggregation of peptide fragments of transthyretin, J. Mol. Biol. 340 (2004) 555–569.
[6] M.D. Benson, The hereditary amyloidoses, Best Pract. Res. Clin. Rheumatol. 17 (2003) 909–927.
[7] A. Gustavsson, U. Engstrom, P. Westermark, Normal transthyretin and synthetic transthyretin fragments form amyloid-like fibrils in vitro, Biochem. Bioph. Res. Co. 175 (1991) 1159–1164.

[8] S.A. Peterson, T. Klabunde, H.A. Lashuel, H. Purkey, J.C. Sacchettini, J.W. Kelly, Inhibiting transthyretin conformational changes that lead to amyloid fibril formation, Proc. Natl. Acad. Sci. U.S.A. 95 (1998) 12956–12960.
[9] P. Christopher, C.E.M. Jaroniec, S. Nathan Astrof, Christopher M. Dobson and Robert G. Griffin, Molecular conformation of a peptide fragment of transthyretin in an amyloid fibril. Proc. Natl. Acad. Sci. U.S.A. 2002, 99 v16748-16753.
[10] P. Christopher, C.E.M. Jaroniec, S. Vikram Bajaj, Michael T. McMahon, Christopher M. Dobson, A. Dobson, Robert G. Griffin, High-resolution molecular structure of a peptide in an amyloid fibril determined by magic angle spinning NMR spectroscopy, Proc. Natl. Acad. Sci. U.S.A. 101 (2004) 711–716.
[11] M. Bucciantini, E. Giannoni, F. Chiti, F. Baroni, L. Formigli, J.S. Zurdo, N. Taddei, G. Ramponi, C.M. Dobson, M. Stefani, Inherent toxicity of aggregates implies a common mechanism for protein misfolding diseases, Nature 416 (2002) 507–511.
[12] J.H. Ippel, A. Olofsson, J. Schleucher, E. Lundgren, S.S. Wijmenga, Probing solvent accessibility of amyloid fibrils by solution NMR spectroscopy, Proc. Natl. Acad. Sci. U.S.A. 99 (2002) 8648–8653.
[13] H. Huang, J. Milojevic, G. Melacini, Analysis and optimization of saturation transfer difference NMR experiments designed to map early self-association events in amyloidogenic peptides, J. Phys. Chem. B. 112 (2008) 5795–5802.
[14] A.T. Petkova, Y. Ishii, J.J. Balbach, O.N. Antzutkin, R.D. Leapman, F. Delaglio, R. Tycko, A structural model for Alzheimer's beta-amyloid fibrils based on experimental constraints from solid state NMR, Proc. Natl. Acad. Sci. U.S.A. 99 (2002) 16742–16747.
[15] X.S.a.E. Giralt, NMR-based methods and strategies for drug discovery, Chem. Soc. Rev. 32 (2003) 365–372.
[16] M. Mayer, B. Meyer, Characterization of ligand binding by saturation transfer difference NMR spectroscopy, Angew. Chem.-Int. Edit. 38 (1999) 1784–1788.
[17] M. Mayer, B. Meyer, Group epitope mapping by saturation transfer difference NMR to identify segments of a ligand in direct contact with a protein receptor, J. Am. Chem. Soc. 123 (2001) 6108–6117.
[18] S. Narayanan, B. Bosl, S. Walter, B. Reif, Importance of low-oligomeric-weight species for prion propagation in the yeast prion system Sup35/Hsp104, Proc. Natl. Acad. Sci. U.S.A. 100 (2003) 9286–9291.
[19] S. Narayanan, B. Reif, Characterization of chemical exchange between soluble and aggregated states of beta-amyloid by solution-state NMR upon variation of salt conditions, Biochemistry 44 (2005) 1444–1452.
[20] J. Milojevic, V. Esposito, R. Das, G. Melacini, Understanding the molecular basis for the inhibition of the Alzheimer's A beta-peptide oligomerization by human serum albumin using saturation transfer difference and off-resonance relaxation NMR spectroscopy, J. Am. Chem. Soc. 129 (2007) 4282–4290.
[21] T.L. Hwang, A.J. Shaka, Water suppression that works. Excitation sculpting using arbitrary wave-forms and pulsed-field gradients, J. Magn. Reson. A 112 (1995) 275–279.
[22] F. Delaglio, S. Grzesiek, G.W. Vuister, G. Zhu, J. Pfeifer, A. Bax, NMRPipe — a multidimensional spectral processing system based on UNIX pipes, J. Biomol. NMR. 6 (1995) 277–293.
[23] S.P. Rucker, A.J. Shaka, Broad-band homonuclear cross-polarization in 2D NMR using DIPSI-2, Mol. Phys. 68 (1989) 509–517.
[24] P. Mesquida, C.K. Riener, C.E. MacPhee, R.A. McKendry, Morphology and mechanical stability of amyloid-like peptide fibrils, J. Mater. Sci.-Mater. Med. 18 (2007) 1325–1331.
[25] T.P. Knowles, A.W. Fitzpatrick, S. Meehan, H.R. Mott, M. Vendruscolo, C.M. Dobson, M.E. Welland, Role of intermolecular forces in defining material properties of protein nanofibrils, Science 318 (2007) 1900–1903.
[26] I. Cardoso, C.S. Goldsbury, S.A. Muller, V. Olivieri, S. Wirtz, A.M. Damas, U. Aebi, M.J. Saraiva, Transthyretin fibrillogenesis entails the assembly of monomers: a molecular model for in vitro assembled transthyretin amyloid-like fibrils, J. Mol. Biol. 317 (2002) 683–695.
[27] O. Hosoya, S. Chono, Y. Saso, K. Juni, K. Morimoto, T. Seki, Determination of diffusion coefficients of peptides and prediction of permeability through a porous membrane, J. Pharm. Pharmacol. 56 (2004) 1501–1507.
[28] K.L. Yam, D.K. Anderson, R.E. Buxbaum, Diffusion of small solutes in polymer-containing solutions, Science 241 (1988) 330–332.
[29] J.T. Keeler, Understanding NMR Spectroscopy, John Wiley & Sons, Inc., New Jersey, 2005.
[30] D.S. Wishart, B.D. Sykes, F.M. Richards, The chemical shift index — a fast and simple method for the assignment of protein secondary structure through NMR-spectroscopy, Biochemistry 31 (1992) 1647–1651.
[31] Andrew J. Baldwin, J.A.-C. Tuomas Spencer, P.J. Knowles, G. Lippens, J. Christodoulou, Paul D. Barker, Christopher M. Dobson, Measurement of amyloid fibril length distributions by inclusion of rotational motion in solution NMR diffusion measurements, Ang. Chem. Int. Ed. 47 (2008) 3385–3387.
[32] Y.S. Wang, D.J. Liu, D.F. Wyss, Competition STD NMR for the detection of high-affinity ligands and NMR-based screening, Magn. Reson. Chem. 42 (2004) 485–489.